Materials Research Express

PAPER • OPEN ACCESS

The effect of natural fibres template on the chemical and structural properties of Biphasic Calcium Phosphate scaffold

Materials Research Express

OPEN ACCESS

RECEIVED
17 February 2020

REVISED
23 May 2020

ACCEPTED FOR PUBLICATION
4 June 2020

PUBLISHED
10 June 2020

PAPER

The effect of natural fibres template on the chemical and structural properties of Biphasic Calcium Phosphate scaffold

Mazen Alshaaer[1,2], Essam Abdel-Fattah[1,3], Iyad Saadeddin[4], Feras Al Battah[5], Khalil Issa[6] and Ghassan Saffarini[4]

[1] Physics Department, College of Science and Humanities in Al-Kharj, Prince Sattam Bin Abdulaziz University, Al-Kharj 11942, Saudi Arabia
[2] Geobiosciences, Geotechnologies and Geoengineering Research Center, University of Aveiro, Campus de Santiago, 3810-193, Aveiro, Portugal
[3] Physics Department, Faculty of Science, Zagazig University, Zagazig, Egypt
[4] Department of Physics, An-Najah National University, Nablus, Palestine
[5] Department of Biology & Biotechnology, Faculty of Sciences, Arab American University, Jenin, Palestine
[6] Orthopedics Unit,Faculty of Medicine and Health Sciences, An-Najah National University, Nablus, Palestine

E-mail: mazen72@yahoo.com

Keywords: tricalcium phosphate, bioceramics, XPS, luffa cylindrical fibre, young modulus

Abstract

Porous biphasic bioceramics that contain hydroxyapatite and tricalcium phosphate were synthesized in this study using luffa cylindrical fibres (LCF) as the template. In addition to improving the pore structure, using this template led to a chemical coating of the pores´ internal surfaces by important minerals such as magnesium and phosphorous from the LCF residue. Evaluation of our preliminary results suggests promising applications in bone tissue engineering. The synthesized porous bioceramics were characterized in view of their microstructural, physical, and *in vitro* features. They showed a trimodal pore system comprising a nano-pore network, smaller macropore with diameters of 5 to 100 μm, and cylindrical macropores with diameters from 100 to 400 μm; and 75% of interconnected porosity was confirmed by Mercury intrusion porosimetry and SEM images. Enhanced cell adhesion of the internal pore surfaces generated long and extended cells inside the macropores. SEM images show how the cells adhered to bioceramic surfaces and developed cytoplasmic extensions. Their proliferation *in vitro* demonstrates that the scaffold architecture and mineral composition are suitable for mesenchymal stem cell seeding and growth.

1. Introduction

Scaffold design and synthesis is a key branch of bone tissue engineering, taking into account the microstructure, architecture and chemical composition of products. The scaffolds must be biodegradable, osteoconductive, biocompatible, and should have physical and mechanical properties that make them appropriate for regenerating tissues [1, 2]. At present, the foremost materials used to manufacture scaffolds are calcium phosphates, bone cement and composite materials [3–7].

Bioactive inorganic minerals and products can interact with physiological liquids to produce strong bonds with the bone matrix by forming layers of fibre-like hydroxyapatite, which in turn interacts with bone tissue and the surfaces of materials [2–4]. Bonding with bone calls for a bioactive mineral layer on the interface of the bone/material [6–8]. Previous studies [9, 10] show that open pore structures (micro-channels) embedded in scaffolds play a vital function in nutrient supply, cell growth, and cell proliferation. The 3D pore network of the scaffolds must provide adequate nutrients and an exchange of gases to stimulate regular cell growth [11–14]. A perfect scaffold would have open pores with physical characteristics suited for bone growth and regeneration.

From a morphological standpoint, scaffolds must feature adequate porosity. A well-developed network of interconnected pores over 100 μm will promote cell penetration [15, 16]. Other desired features are: controlled bioactivity, a bio-resorbability rate compatible with the spontaneous bone regeneration rate, mechanical

behaviour comparable to that of natural bone, and a porous network suitable for cell penetration, formation of blood vessels, and tissue ingrowth [17]. A fine pore network would favour reduced levels of dissolved oxygen (hypoxic) circumstances and invoke osteochondral arrangement prior osteogenesis, whereas well-vascularized macro-pore structure result in direct osteogenesis, bypassing the development of cartilage [5]. There is a close relationship, however, between scaffold porosity and mechanical properties: a greater scaffold porosity and a larger pore structure lead to reduced mechanical performance. Hence, there is a specific size and structure for functional pore and porosity. A balance should be done in view of the healing rate, re-modeling rate and/or rate of degradation of the scaffold matrix [5], while the scaffold design requires permeability (i.e., pore interconnectivity) for waste discharge and nutrient transfer, and must ensure enough stiffness and strength to hold loads transmitted to the scaffold from the adjusted healthy bone [15].

Most studies suggest a pore structure with diameters vary from 100 μm to 400 μm [3]. Mazali and Alves [18] introduced a template of the vascular network of luffa cylindrical fibres for the production of a porous medium. The authors synthesized calcium phosphates porous ceramic for different applications, particularly medical ones, and found that the template proposed —luffa cylindrical fibres— provided for inorganic replicas on the centimetre scale, too large for bone tissue engineering [3].

Our aim was to improve upon previous work [11] and devise a new methodology for preparing calcium phosphate ceramics with a bimodal pore structure suitable for bone scaffolds. A degradable porous hydroxyapatite scaffold was prepared using the homogeneous outer core of luffa cylindrical fibre (LCF) as the replication method [11]. In this study, a novel structure of porous biphasic calcium phosphate ceramic material was developed, featuring a trimodal pore structure and attractive open cylindrical macropores. We also investigated the contribution of LCF mineral residue as a nutrient reservoir for essential minerals such as Mg and P in the chemical coating of the internal pore surfaces of bioceramics during sintering. The scaffolds were evaluated *in vitro*. Their pore size, geometry, and porosity can be designed by using the required diameter of the LCF, from 100 to 400 μm. Use of this renewable resource material to produce bioceramic scaffolds is spreading worldwide, given its low cost, attractive network structure, the fibre´s geometry, and its diverse range of diameters.

2. Materials and methods

2.1. Porous biphasic calcium phosphate: preparation

Luffa sponge was extracted from dried fruits. In order to obtain the desired pore size (100–400 μm), only the homogeneous outer core was used as the replica. It was cut into discs (diameter 20 mm, thickness 5 mm), which were then washed in warm water several times. Afterwards, these fibre discs were washed with distilled water and dried at 60 °C for one day. Fine dried LCF chips (density 0.375 g cm^{-3}) from 100 to 400 μm in size were prepared and mixed with the luffa fibres to obtain the 3D structure. HA nano-powder was synthesised by means of a chemical precipitation following the following equation:

$$10Ca(NO_3)_2 + 6(NH_4)_2HPO_4 + 8NH_4OH \rightarrow Ca_{10}(PO_4)_6(OH)_2 + 6H_2O + 20NH_4NO_3.$$

Then, 39.5 g of diammonium phosphate was dissolved in deionised water to prepare a 800 ml solution of $(NH_4)_2HPO_4$. Another solution —600 ml $Ca(NO_3)_2$— was prepared by adding 115 g of calcium nitrate tetrahydrate salt in deionised water.

The two solutions were mixed by stirring, dropwise, at temperature varying from 60 °C to 80 °C. The pH of the solution varied from 9 to 10 with the dissolving of ammonium hydroxide. White precipitates of hydroxyapatite produced after the addition of $(NH_4)_2HPO_4$ to the $Ca(NO_3)_2$ solution at a rate of 3 ml min^{-1} under continuous stirring; these precipitates were left at room temperature for 24 h to produce nanostructure HA rods. The nano-powder was rinsed with deionised water until the pH decreased to 7. The precipitates were dried overnight at 80 °C and calcined at 400 °C for 2 h to remove the residual organic compound [11].

Under constant stirring, for 30 min, PVA was dissolved in 20 ml of deionized water, at 60 °C. Then HA powder was added to the solution in small amounts, constantly mixing it at room temperature (RT). When all the powder was wet, the mixture was sonicated for 15 min.

The PVA-HA was mixed with luffa fibres (luffa fibre/HA powder weight ratio of 0.25). The ceramic slurry was dried at 60 °C for 24 h, and then heated step-wise in a furnace at 1 °C min^{-1}, up to 1100 °C and kept at this temperature for 4 h. Finally, the sintered material was cooled slowly until it reached RT.

2.2. Characterization of scaffolds and precursors

The elemental composition of the luffa fibres was determined using Thermo Scientific iCAP 7000 Inductively Coupled Plasma Optical Emission Spectrometer (ICP-OES), (USA). The specimens' morphology were

examined by scanning electron microscopy, (Inspect F50, FEI, USA). The Mesenchymal Stem Cells (MSC) connected to the bioceramics were cleaned with 2 ml of 1X PBS and fixed with 2% gluteraldehyde for one day at 4 °C. After subjecting the scaffolds to graded alcohol dehydrations, they were dried at ambient conditions using filter papers, and sputter-coated with platinum. Matrices without cells served as controls.

The microstructural phases were identified by the X-ray diffraction (XRD) (Shimadzu XRD-6000, Japan) applying CuKα radiation at 20 mA, 40 kV). Scans were performed from 10° to 60° at a rate of 2 °C min^{-1}. The surface chemistry of the obtained bioceramics was characterized by means of x-ray photoelectron spectroscopy: an XPS system (Thermo K Alpha spectrometer, USA).

The pore structure of the scaffolds (1–400 μm) was determined by mercury intrusion porosimetry (PoreMaster, USA). The total porosity (TP) of the scaffold was derived from the bulk density (ρB) or ratio between the sample weight and volume, and the apparent density for the solid fraction (ρo), obtained by Helium-pycnometry. Finally, the compressive strength and the strain were measured using a CBR tester (Controls, Italy).

2.3. In vitro characterization of scaffolds

The MSC cell isolation, osteogenic differentiation, and cell seeding on the scaffolds were described in our previous study [11].

2.3.1. MSC cell isolation

The MSCs were isolated from human bone marrow aspirates by means of density gradient centrifugation. The cells were expanded in non-differentiating MSC growth medium (CCM) containing α-minimal essential medium (α-MEM), 10% fetal bovine serum (FBS), 1% penicillin-streptomycin (PEN-STREP), and 2 mM glutamine. The cells were incubated at 37 °C with 5% CO_2. Once they reached 90% confluence, they were harvested by rinsing with 0.25% trypsin and 0.03% EDTA solution. At that point they underwent a second passage until they reached 80% confluence, and were trypsinized and cryopreserved in liquid nitrogen. These cells were designated as passage 1 (P1) cells.

2.3.2. Osteogenic differentiation

The cells were seeded in 12 multi-well plates for an estimated 80% confluence. Each experiment comprised 12 cultures: 6 under osteogenic conditions, and 6 controls under normal cell culture conditions. In order to induce osteogenic differentiation of the MSCs, the cultures were maintained in osteogenic media consisting of 60 μM ascorbic acid, 10 mM β-glycerol phosphate, and 100 nM dexamethasone. The medium was changed every 2–3 days. After 21 days of differentiation experiments (with and without osteogenic media), the cells were evaluated via Alizarin Red Staining (ARS) and silver nitrate.

2.3.3. Cell seeding on the scaffolds

The cryopreserved (P1) cells were re-plated at a seeding density of 4000 cells/cm2 in alpha MEM as described above. At near confluency, P2 cells were harvested with 0.25% trypsin in EDTA and re-suspended at a density of 2×105 cells/ml alpha-MEM plus 1% penicillin/streptomycin. After sterilizing the calcium phosphate scaffolds in 70% ethanol for 24 h, they were incubated with cell culture media containing 10% FBS for at least 4 h. The MSCs were seeded into the scaffolds at a density of 200,000 cells/per scaffold. The MSCs were cultured with osteogenic medium and cell culture medium as a standard control to verify their proliferative and differentiation potential at 37 °C and 5% CO_2 for 4 weeks. The medium was changed every 3–4 days.

3. Results and discussion

3.1. Porous calcium phosphate ceramics

In the present study, nanopowder of fibre-like calcium deficient hydroxyapatite (CDHA), which is similar to osteoconductive hydroxyapatite, was prepared following a homogeneous precipitation method [11]. The SEM image of the synthesized CDHA can be seen in figure 1(A). The produced fibre-like hydroxyapatite has a length of approximately 250 nm and a diameter of some 50 nm. The molar ratio of Ca/P is about 1.65, while the standard ratio is 1.67 (see figure 1(B)). Reducing the calcium ratio increases the bioactivity of this mineral [10]. Fibrous hydroxyapatite is known to exhibit high strength due to a synergy of the fibres, toughness, and pullout characteristics [19].

As depicted in figure 2, the corresponding XRD pattern to the calcium phosphate nano-powder resembles the crystalline hydroxyapatite. Yet the XRD peak locations became sharper as a result of manufacturing bio-scaffolds by annealing at 1100 °C (figure 2, upper). New XRD peaks appeared reflecting TCP and the formation of biphasic calcium phosphates (HA and TCP). This sharpness in the XRD peaks indicates the formation of large

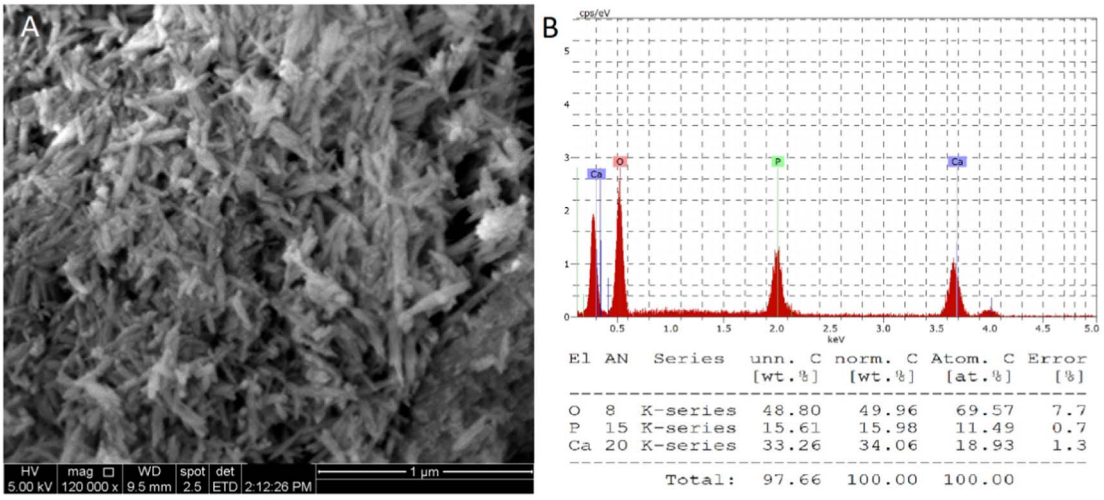

Figure 1. SEM image (A) and EDX analysis (B) of calcium-deficient hydroxyapatite nano-particles.

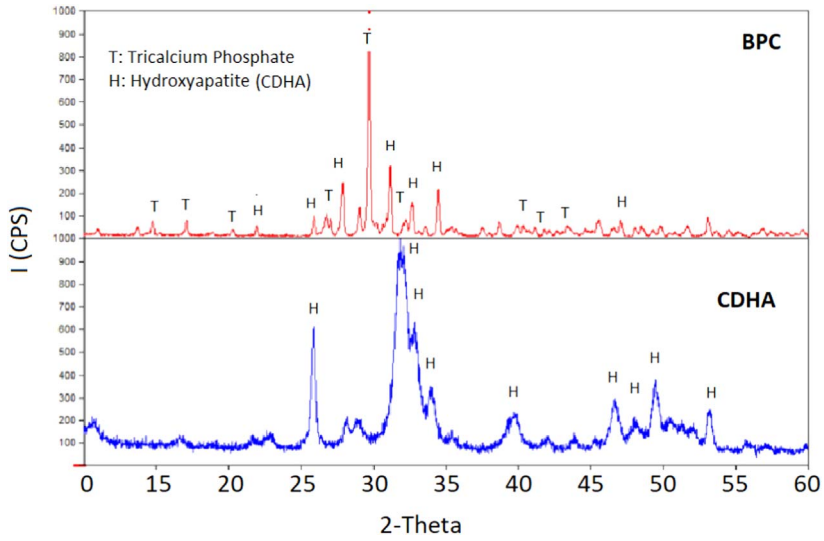

Figure 2. X-ray diffraction patterns of fibre-like hydroxyapatite nano-powder (lower), and biphasic calcium phosphate (upper).

sintered hydroxyapatite and tricalcium phosphate, a close-up of these grains being shown in the SEM image of figure 3. The microstructure of the scaffold composition reveals homogeneous and sintered hydroxyapatite and TCP grains as well as nanopores (figure 3(b)). SEM images of the inner pores of the CaP scaffold show high porosity (above 70%), the pore structure varying from 100 μm to 500 μm. The interconnection of the pores is visible in figure 4.

Sintering the scaffold at 1100 °C for 2 h led to a dramatic change in the calcium phosphate grain (HA and TCP) morphology: along with grain growth (figure 3), sintering caused the cement particles to join together. At the same time, equal-axed hydroxyapatite and tricalcium phosphate grains formed even though macropores remained in the structures (figure 4). The presence of β-TCP in the sintered scaffold at 1100 °C would indicate some extent of thermal decomposition of the HA, into the TCP (figure 2). All these phases conform a group of reactive biomaterials.

3.2. Pore structure

The homogenous, treated outer cores of luffa cylindrical fibres have diameters around 100 to 400 μm and are well connected (figure 5), fulfilling the requirements [11, 15] for use as a template for a bioceramic scaffold. The cylindrical natural fibres are seen to have rough surfaces.

In sum, the sintered bioceramics composed mainly from HA and TCP phases with macropore structure (as a replica of the fibres in the LCF), and smaller open pores in the matrix. Such a design for bioceramic scaffolds,

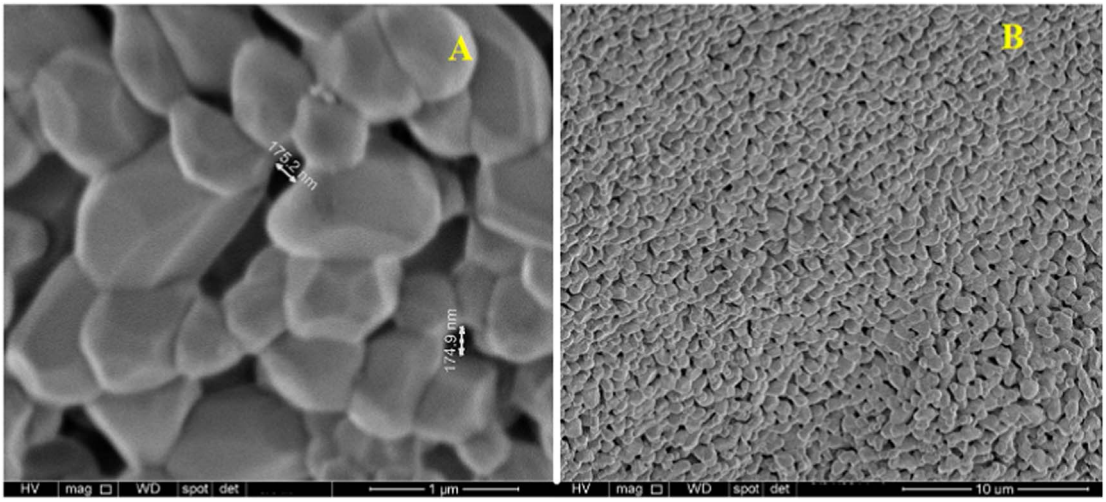

Figure 3. SEM image of sintered BPC-based scaffold after annealing at 1100 °C.

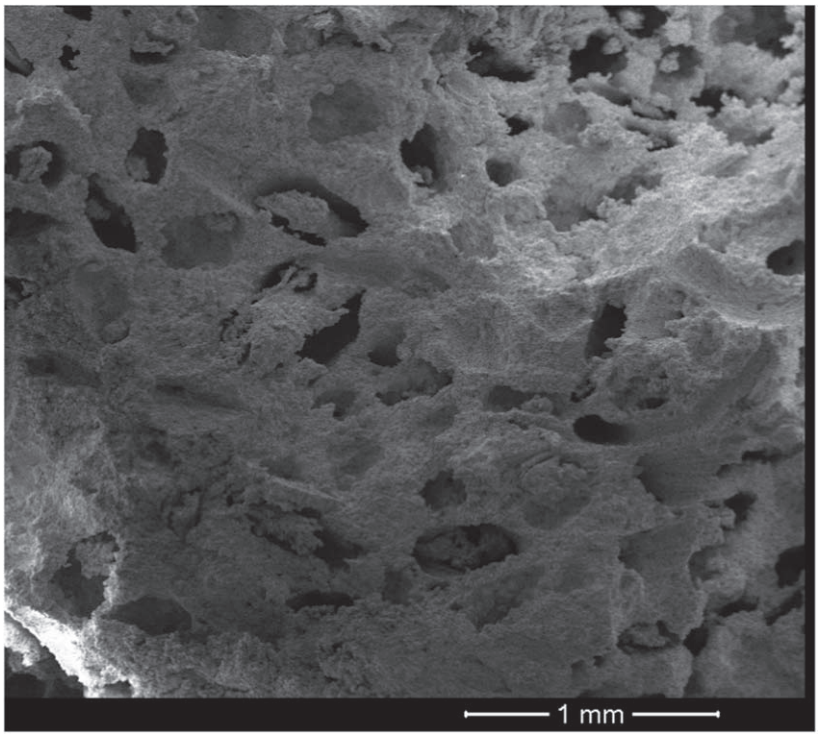

Figure 4. SEM micrograph of the inner pores of the bioceramic scaffold.

with enhanced connectivity and highly effective porosity, can facilitate the mass transfer of oxygen and nutrients for cell growth, as well as the discharge of waste [20–22].

Pore interconnectivity primarily comes from the connected LCF mat and the contact point between ceramic grains (figure 3), but also depends on the formation of the fine pore structure under 5 μm in diameter that is produced by the phase conversion mechanism [21].

To verify the surface morphology performed using SEM, a study of pore structure characteristics was undertaken, involving MIP. Figure 6 shows a bimodal distribution of pore size: pores just a few micrometres in diameter are found along with macropore structure with diameters of hundreds of micrometres. The total open porosity is around 75% of the scaffold bulk structure (figure 6(A)). Some 60% of the porosity is from the smaller pores (~diameters from 1 to 100 μm), whereas 40% is from larger pores (100 to 200 μm). In this context, large macropores can accommodate osteoblasts and undifferentiated bone mesenchymal stem cells, whereas smaller

Figure 5. SEM micrographs of luffa fibres.

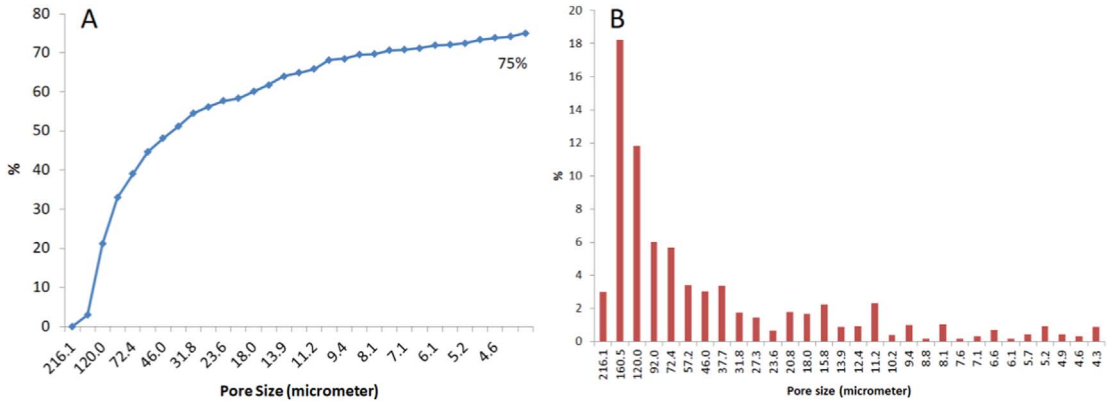

Figure 6. Mercury intrusion porosimetry of the bioceramic scaffold: (a) cumulative pore size distribution and (b) incremental pore size.

pores serve as bridges connecting adjacent macropores, promoting nutrient and metabolite exchange [11, 22, 23].

3.3. The chemical incorporation of luffa cylindrical fibre

Previous studies [18, 24] report that a full decomposition/evaporation of LCF takes place at around 600 °C, leaving a pure inorganic matrix. The degradation reactions and evaporation of the LCF organic components occur at the sintering temperature [18]. As illustrated in figure 7, there are three main loss regions in the TGA curve of LCF, representing a mass loss of 75.7%. The first mass loss peak is related to the evaporation of water, entailing a mass loss of around 6%. The subsequent events represent ~70%, attributed to pyrolysis of the LCF. The thermal decomposition of the LCF is completed at 440 °C, and leaves a powder, with residual carbon [18]. Thermal decomposition at 800 °C leaves a fine white residue consisting of Sodium, Calcium, Magnesium, and Iron (table 1). The presence of calcium and magnesium makes the residue of LCF appropriate for bone growth, since deficiencies in these elements can cause abnormal bone development [3–5].

The surface chemical composition derived from the BPC scaffold was investigated using XPS. The survey spectra of the sample show photoelectron peaks of Phosphor P2p, Calcium Ca2p, Oxygen O1s, and magnesium Mg1s at respective binding energies around 138.11 eV, 351.95 eV, 535.03 eV and 1306.7 eV. The atomic relative weight in the sample is given in figure 8.

The significant difference between the composition of the original BPC scaffold, with CDHA and TCP, and the scaffold surface material is a strong indication of how the incorporation of LCF mineral residue in the bio-

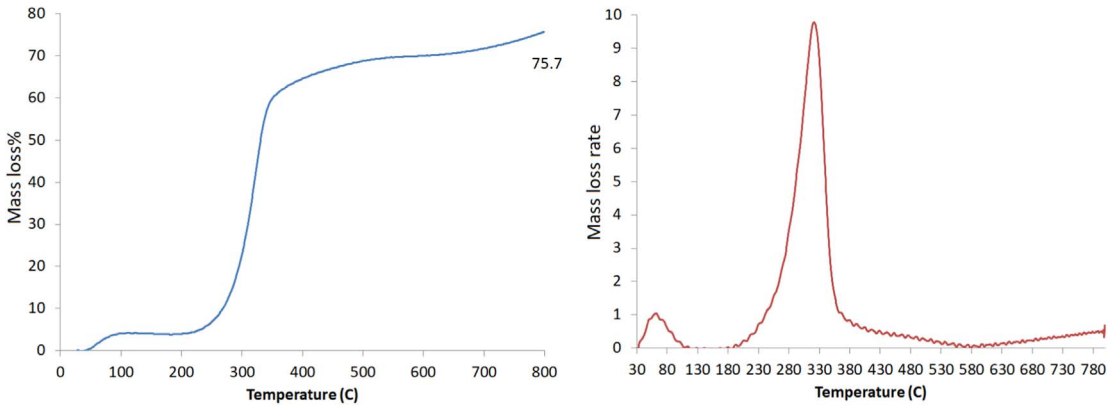

Figure 7. TGA analysis of LCF.

Table 1. Mineral composition of raw LCF (obtained by the ICP technique).

Minerals	mg/1000 g
Na	7191
Fe	42
Mg	431
Ca	2849

chemical composition of the scaffold can surface during the sintering process. The chemical contribution of the LCF residue in the BPC is a result of LCF mineral diffusion into the surfaces of the scaffold. This effect is evident in two areas: new elements in the ceramic surface, such as magnesium, in reasonable quantities, as well as a decreased ratio of calcium to phosphorus as compared to the origin phases (HA and TCP). Although Mg was not added at any stage of the scaffold preparation, its presence on the surface nearly matches that of phosphorus. The logical explanation would be that this element comes from the LCF residue (see table 1), and diffuses the BPC surface during sintering. Magnesium is an essential element in bone minerals, providing a sound biochemical environment for stem cell growth and differentiation. Its diffusion to the scaffold surface therefore plays a key role in increasing bioactivity and ensuring necessary nutrients for the cells. The other major finding is the reduced Ca/P molar ratio. In the BPC scaffold it ranges from 1.5 (TCP) to 1.65 (CDHA), but it drops sharply to less than 1 (see figure 8). The P from the LCF residue (table 1) was incorporated into the scaffold surface and led to a marked deficiency in Ca with respect to the matrix of BPC. This Ca deficiency at the scaffold surface means greater bioactivity of the material and interaction with the cells and tissues [5].

3.4. Mechanical characterisation

One of the crucial characteristics of suitable bone substitute is its mechanical behaviour, which should closely match that of the natural bone tissues. Mechanical characteristics, i.e. the strength and the stiffness, are important considerations when attempting to reproduce the appropriate response of load-bearing natural bone. Introducing biopolymers become widespread for the providing of biodegradable strengthening for bone tissue applications [8]. Yet their low mechanical performance largely limit their employment to specific applications.

Figure 9 displays the typical linear part of the stress-strain response of the produced bioceramic scaffold. The compressive strength and the elastic modulus of the scaffold are 3.7 MPa and ~50 MPa respectively. Given that the mechanical, biological and physical properties of the porous ceramics lie within the range of those of spongy bone [10], this can be considered a promising material for bone tissue regeneration.

3.5. Preliminary evaluation of biocompatibility of scaffolds

The final step of our study involved preparing the BPC scaffold for *in vitro* cultivation. MSCs were added to the 3D porous bioceramic-based scaffold with an osteogenic medium for 20 days. After that, new tissue masses occupied the macropores, as shown by SEM (figure 10). The scaffold visually illustrated the presence of cells and tissues on surfaces within the open macropore channels. Figures 10(A) and (B) show cells attached to the scaffold surface: cell adhesion gave rise to highly stretched cells within the macropore network.

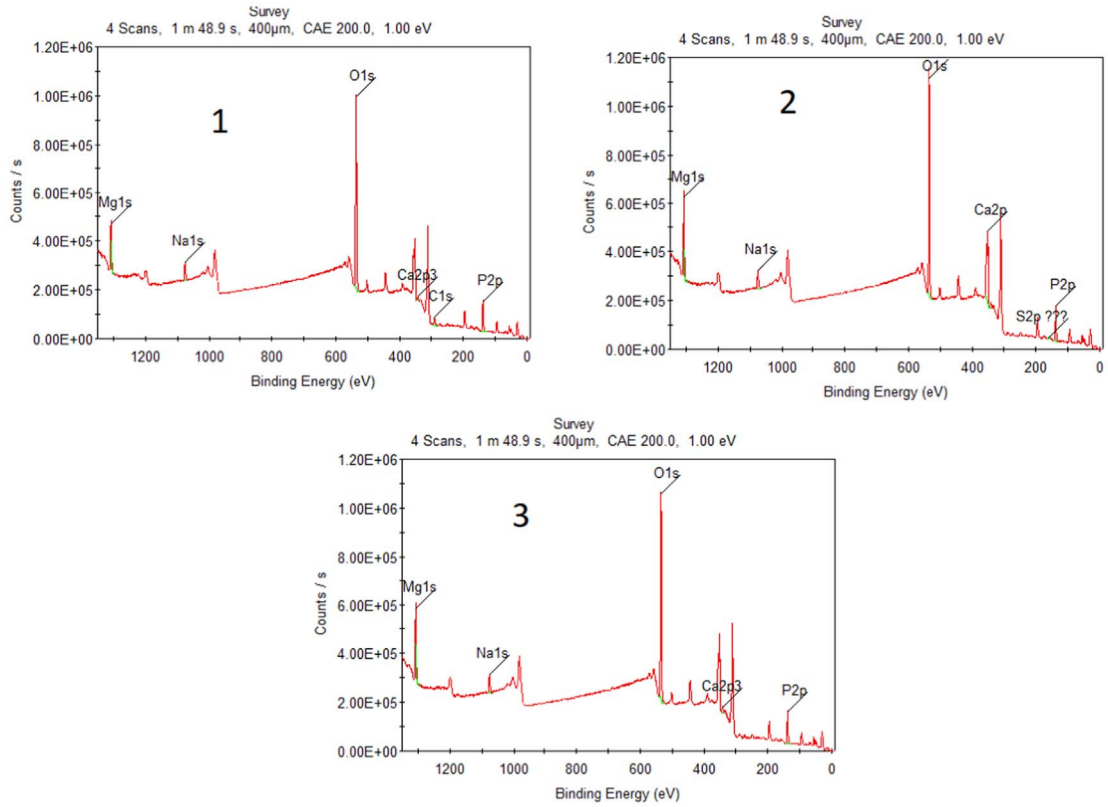

Element	Point 1 Peak BE	Point 1 Atomic %	Point 2 Peak BE	Point 2 Atomic %	Point 3 Peak BE	Point 3 Atomic %
O 1s	535.03	58.5	535.19	68.59	536.03	64.3
Mg 1s	1306.7	9.35	1306.82	8.83	1306.96	4.71
Ca 2p	351.95	13.93	342.27	1.19	342.71	0.62
P 2p	138.11	15.23	138.23	18.02	139.07	16.47
Na 1s	1074.94	2.55	1075.23	3.37	1075.29	2.99
S 2p	159.51	0.45				

Figure 8. Relative surface atomic concentration of elements in the bioceramics (XPS surface analysis of three random areas).

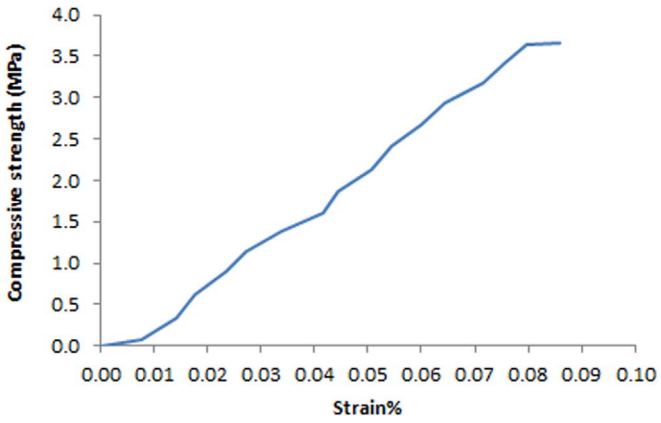

Figure 9. Stress-strain curve of the BPC scaffold.

The cells moreover adhered to the BPC and developed cytoplasmic extensions, visible in figure 10(B), whose proliferation in the culture comes to demonstrate that the bioceramic scaffold design was appropriate for MSC growth. The increased porosity and interpore connectivity of the biomaterial favours high density and multiple

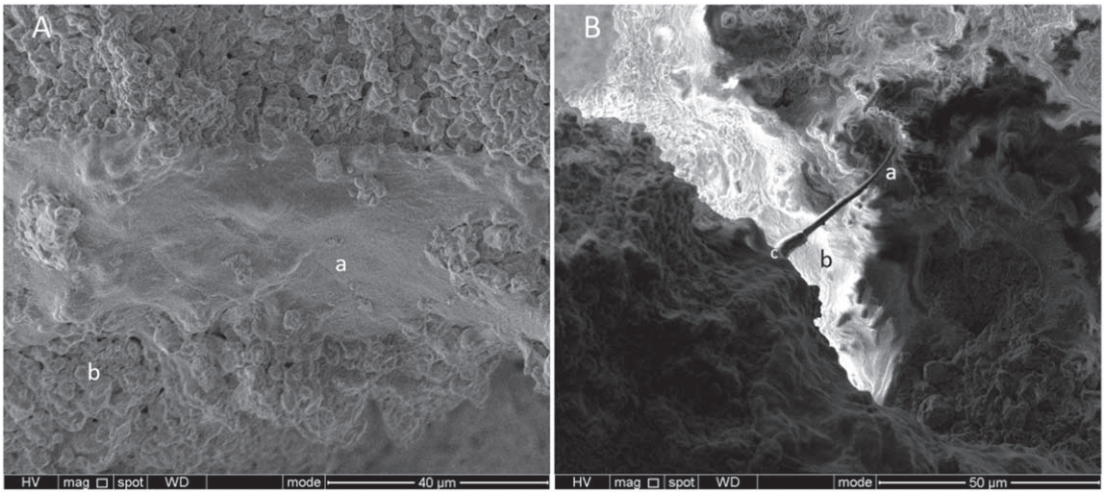

Figure 10. SEM micrographs showing: (A) an osteoblast cell attached to the surface of the bioceramic scaffold, and (B) formation of new bone tissue, as the cellular processes extend over the underlying scaffold matrix with.

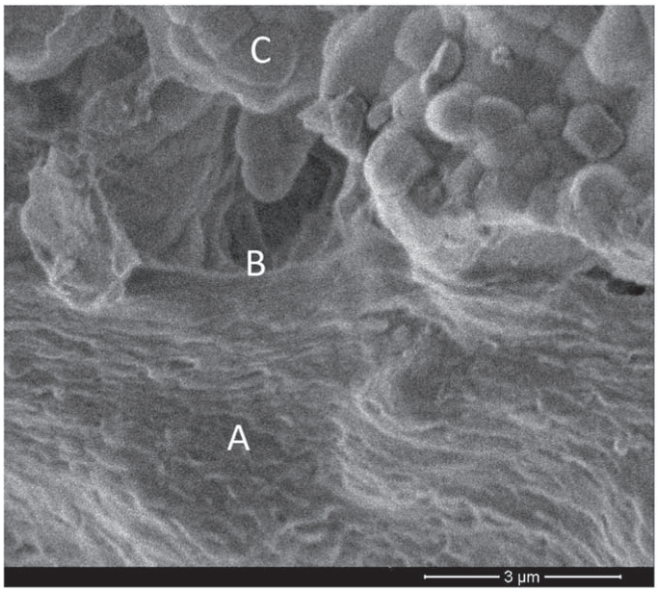

Figure 11. Adhesion (B) of tissue cell (A) on scaffold-matrix (C).

layers of cells. The newly forming bone tissue follows the outline of the bioactive BPC surface, while the bone mineralogical phase composed from HA and TCP crystals. The scaffold surface contains high proportions of Mg, Ca and other minerals from the LCF residue (see figure 8), factors which give significant indications of osteogenic differentiation.

One of the most major rules of scaffolds for cell transplantation is their ability to support cell adhesion. The adhesion characteristic is mainly attributed to the physical and chemical properties of the surface [25]. The characterization of cell morphology and adhesion were performed using SEM. The cells appear elongated and horizontally spread out on scaffold, figure 10(A). Migrating cells exhibit surface characteristics that indicates to the development of cytoplasmic extensions and membrane projections, figure 10(B) (point a). This cytoplasmic distribution of cells suggesting that scaffold permit cellular infiltration, critical for tissue regeneration [26–28].

Cell adhesions have been found to facilitate interactions between the tissue cells and the scaffold as reported in figure 11 [27]. It is reported that tissue cells mainly interact with the scaffold surface indicating a strong interaction between cells and the bio-matrix. This result is in good agreement with the fact that cells adherence during the culture and suggests that the contact with the scaffold was functional.

4. Conclusions

The present study investigates the suitability of luffa cylindrical fibre (LCF) for achieving sound structural and chemical properties in BCP porous ceramics. We prepared a degradable porous BPC scaffold using the homogeneous outer core of LCF as the replication method. In addition to attaining high pore interconnectivity with acceptable mechanical properties with this method, LCF was found to serve as a nutrient reservoir for the bioceramics. The resulting bioceramic material, featuring a novel trimodal pore structure, fulfils porosity needs while exhibiting enough mechanical performance for load-bearing applications; furthermore, the surface benefits from important minerals, e.g. magnesium, derived from the residue of LCF burnt during the sintering process.

The method effectively produced porous biphasic calcium phosphate ceramics with a trimodal pore structure (nanopores and macropores ranging from 70 to 400 μm, and finer macropores of diameter 10 to 30 μm), and 75% of open porosity. Preliminary *in vitro* characterization demonstrates the formation of new bone tissue, as the cellular processes extend over the underlying scaffold matrix with cytoplasmic extensions. The macropores of this structure can accommodate undifferentiated MSCs and osteoblast bone cells, while the smaller pores serve as bridges between adjacent macropores, promoting nutrient and metabolite transfer. The ceramic surfaces hosting the cells and tissues were found to contain essential minerals needed for healthy bone tissue growth, such as magnesium and phosphorous. Finally, the elastic modulus of the bioceramic scaffold is ~50 MPa. Because the mechanical and physical properties of the bioceramic scaffold lie within the range of those of natural spongy bones, these findings point to a scaffold material with great potential for hard tissue regeneration.

In vitro assays showed that cells attached to the apatite crystals making up the scaffold matrix, and that the cells adhering to the ceramic surfaces developed cytoplasmic extensions. Therefore, the scaffold architecture proved suitable for MSC seeding and growth, key factors for osteogenic differentiation.

Based on the above, we may underline that LCF holds substantial promise for improving the biological surface characteristics of ceramics for bone tissue engineering. However, this new finding calls for further verification, and merits further study, as it could be an important breakthrough for the preparation of scaffolds and bioceramics having excellent characteristics and involving low cost.

Acknowledgments

This project was supported by the Deanship of Scientific Research (Specialized Research Grant program) at Prince Sattam Bin Abdulaziz University under the research project #2019/01/10964.

ORCID iDs

Mazen Alshaaer https://orcid.org/0000-0001-5657-5418

References

[1] Ghosh R, Sarkar R and Paul S 2006 Development of machinable hydroxyapatite-lanthanum phosphate composite for biomedical applications *Mater. Des.* **106** 161–9
[2] Hench L L and Polak J M 2002 Third-generation biomedical materials *Science* **295** 1014–7
[3] Gerhardt L and Boccaccini A R 2010 Bioactive glass and glass-ceramic scaffolds for bone tissue engineering *Materials* **3** 3867–910
[4] Sheikh Z, Zhang Y L, Grover L, Merle G E, Tamimi F and Barralet J 2015 *In vitro* degradation and *in vivo* resorption of dicalcium phosphate cement based grafts *Acta Biomater.* **26** 338–46
[5] Zhang J, Liu W, Schnitzler V, Tancret F and Bouler J 2014 Calcium phosphate cements for bone substitution: chemistry, handling and mechanical properties *Acta Biomateriala* **10** 1035–49
[6] Bergemann C, Cornelsen M, Quade A, Laube T, Schnabelrauch M, Rebl H, Weißmann V, Seitz H and Nebe B 2016 Continuous cellularization of calcium phosphate hybrid scaffolds induced by plasma polymer activation *Materials Science and Engineering* C **59** 514–23
[7] Shanglong X, Dichen L, Bingheng L, Yiping T, Chaofeng W and Zhen W 2007 Fabrication of a calcium phosphate scaffold with a three dimensional channel network and its application to perfusion culture of stem cells *Rapid Prototyping Journal* **13** 99–106
[8] Almeida J C, Wacha A, Gomes P S, Alves L C, Fernandes M H V, Salvado M H R and Fernandes M H R 2016 A biocompatible hybrid material with simultaneous calcium and strontium release capability for bonetissue repair *Materials Science and Engineering* C **62** 429–38
[9] Ochoa I, Sanz-Herrera J A, García-Aznar J M, Doblaré M, Yunos D M and Boccaccini A R 2009 Permeability evaluation of 45S5 Bioglass®-based scaffolds for bone tissue engineering *J. Biomech.* **42** 257–60
[10] Alshaaer M, Kailani M H, Jafar H, Ababneh N and Awidi A 2013 Physicochemical and microstructural characterization of injectable load-bearing calcium phosphate scaffold *Adv. Mater. Sci. Eng.* **2013** 149261
[11] Alshaaer M, Kailan M H, Ababneh N, Abu Mallouh S A, Sweileh B and Awidi A 2017 Fabrication of porous bioceramics for bone tissue applications using luffa cylindrical fibres (LCF) as template *Processing and Application of Ceramics* **11** 13–20

[12] Zhou H, Lawrence J G and Bhaduri S B 2012 Fabrication aspects of PLA–CaP/PLGA–CaP composites for orthopedic applications: a review *Acta Biomaterials* **8** 1999–2016
[13] Tamimi F, Le Nihouannen D, Eimar H, Komarova S, Sheikh Z and Barralet J 2012 The effect of autoclaving on the physical and biological properties of dicalcium phosphate dihydrate bioceramics: brushite versus monetite *Acta Biomaterials* **8** 3161–9
[14] Liu W, Zhang J, Rethore G, Khairoun K, Pilet P, Tancret F, Bouler J and Weiss P 2014 A novel injectable, cohesive and toughened Si-HPMC (silanized-hydroxypropyl methylcellulose) composite calcium phosphate cement for bone substitution *Acta Biomaterials* **10** 3335–45
[15] Pilliar R M, Kandel R A, Grynpas M D, Theodoropoulos J, Hu Y, Allo B and Changoor A 2016 Calcium polyphosphate particulates for bone void filler applications *Biomedical Materials Research Part B: Applied Biomaterials* **105B** (4) 874-884
[16] Genovese K 201 Three-dimensional microscopic deformation measurements on cellular solids *J. Mech. Behav. Biomed. Mater.* **60** 78–92
[17] Akhtar N, Saeed A and Iqbal M 2003 Chlorella sorokiniana immobilized on the biomatrix of vegetable sponge of Luffa cylindrica: a new system to remove cadmium from contaminated aqueous medium *Bioresour. Technol.* **88** 163–5
[18] Mazali I O and Alves O L 2005 Morphosynthesis: high fidelity inorganic replica of the fibrous network of loofa sponge (Luffa cylindrica) *Anais da Academia Brasileira de Ciências* **77** 25–31
[19] Burg K J L, Porter S and Kellam J F 2000 Biomaterial developments for bone tissue engineering *Biomaterials* **21** 2347–59
[20] Sheikh Z, Geffers M, Christel T, Barralet J and Gbureck U 2015 Chelate setting of alkali ion substituted calcium phosphates *Ceram. Int.* **41** 10010–7
[21] Lertcumfu N, Jaita P, Manotham S, Jarupoom P, Eitssayeam S, Pengpat K and Rujijanagul G 2016 Properties of calcium phosphates ceramic composites derived from natural materials *Ceram. Int.* **42** 10638–44
[22] Zhou H, Kong S, Liu, Pan Y, Liu Y, Luo M and Deng L 2016 Fabrication and evaluation of calcium alginate/calcium polyphosphate composite *Mater. Lett.* **180** 184–7
[23] Russias J, Saiz E, Nalla R K, Gryn K, Ritchie R O and Tomsia A P 2006 Fabrication and mechanical properties of PLA/HA composites: a study of *in vitro* degradation *Materials Science and Engineering* C **26** 1289–95
[24] Tanobe V O A, Sydenstricker T H D, Munaro M and Amico S C 2005 A comprehensive characterization of chemically treated Brazilian sponge-gourds (Luffa cylindrica) *Polym. Test.* **24** 474–82
[25] Bacakova L, Filova E, Parizek M, Ruml T and Svorcik V 2011 Modulation of cell adhesion, proliferation and differentiation on materials designed for body implants *Biotechnol. Adv.* **29** 739–67
[26] O'Brien F J, Harley B A, Waller M A, Yannas I V, Gibson L J and Prendergast P J 2007 The effect of pore size on permeability and cell attachment in collagen scaffolds for tissue engineering *Technol. Health Care* **15** 3–17
[27] Tsuruga E, Takita H, Itoh H and Hollister S J 2005 Porous scaffold design for tissue engineering *Nat. Mater.* **4** 518–24
[28] Guarino V and Ambrosio L 2008 The synergic effect of polylactide fiber and calcium phosphate particle reinforcement in poly e-caprolactone-based composite scaffolds *Acta Biomaterials* **4** 1778–87